

DFTT 24/2001
FISIST/12-2001/CENTRA
28 August 2001

INCLUSIVE DENSITY OF SECONDARIES IN HEAVY ION COLLISIONS

J.Dias de Deus and Yu. M. Shabelski*

CENTRA, Instituto Superior Técnico, 1049-001 Lisboa, Portugal

R. Ugoccioni

Dipartimento di Fisica Teorica and INFN – Sezione di Torino, 10134 Torino, Italy

ABSTRACT

The inclusive density of charged secondaries produced in high energy heavy ion collisions are calculated in the framework of multiple scattering theory and quark-gluon string model. The obtained results are in agreement with the data only assuming rather large inelastic screening/percolation effects. We predict the total saturation of relative inclusive densities in dependence on the number of interacting nucleon. Predictions for LHC are also given.

*Permanent address: Petersburg Nuclear Physics Institute, Gatchina, St.Petersburg, Russia

E-mail: shabelsk@thd.pnpi.spb.ru

1. Introduction

The processes of high energy heavy ion collisions can be considered in the framework of multiple scattering theory. Many references can be found in reviews [1, 2, 3, 4]. Contrary to the case of hadron-nucleus interactions, in the case of heavy ions it is impossible to sum analytically¹ the contributions of all diagrams of Glauber approach.

However, the contributions of the most important diagrams can be accounted for analytically, that allows one to calculate the integral cross sections of different processes, distributions on the number of interacting nucleons, multiplicities of secondaries and their inclusive distributions in reasonable agreement with the data.

It is well-known that in high energy hadron-nucleus collision there exists inelastic screening [6, 7] which is confirmed experimentally, especially for the case of hadron-deuteron interactions. The same inelastic screening should exist in high energy heavy ion collision. This effect is very small for integrated cross sections (because many of them are determined by geometry), but it is very important [8] for the calculations of secondary multiplicities and inclusive densities. Similar results can be obtained [9, 10] in the framework of string fusion [11], or percolation [12] models where string fusion/percolation effects directly correspond [13] to the pomeron interactions.

In the present paper we will give the theoretical estimations for relative inclusive densities, integrated multiplicities and rapidity distributions using both Gribov's reggeon diagram technique [14] and percolation approach as well as Quark-Gluon String Model (QGSM) [15, 16].

We will also compare the above estimates with results from the Dual String Model (DSM) [9, 17] and find them remarkably similar, although the DSM is based on a different approach: it takes as input quantities measured in $p\bar{p}$ and/or pp collisions, and screening is realised via fusion of strings exchanged in partonic sea collisions, which can lead to percolation effects [18].

We will show that there exists a qualitative difference between secondary production at CERN SpS and RHIC energies and this difference can be described only by accounting for rather large inelastic screening/percolation/string fusion effects. These effects decrease the inclusive density about two times, that is in agreement with previous estimations [8].

For the distributions calculated in the present paper in DSM it is string fusion that leads to saturation with the number of participant nucleons, percolation phase transition is not felt.

2. Spectra of secondaries and multiplicities in heavy ion collisions

We start with standard multiple scattering theory consideration without inelastic screening. At high energies the spectrum of a secondary particle h produced in the central rapidity region of nucleus A - nucleus B collision is proportional to the same

¹It can be done with the help of Monte Carlo calculation of multidimensional integral [5].

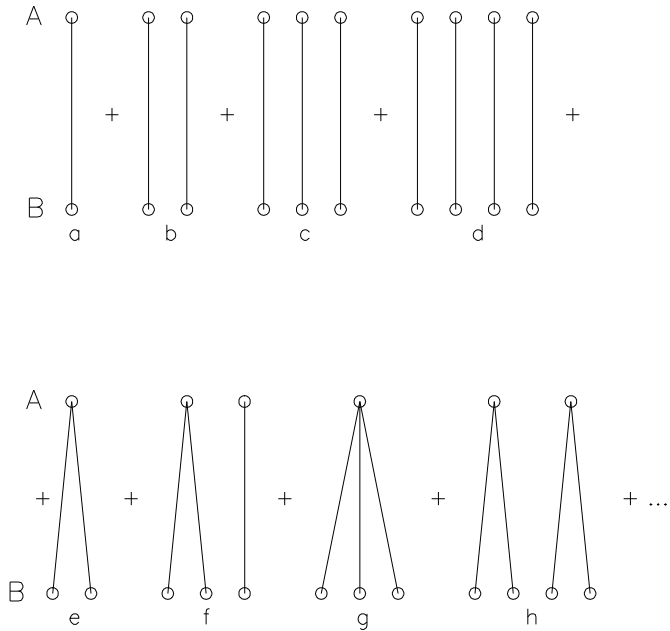


Fig. 1

Figure 1: Diagrams corresponding to the rigid target approximation for nucleus A – nucleus B interaction. Only interacting nucleons are shown as the open points.

spectrum in NN collision [19]

$$\frac{d\sigma(AB \rightarrow hX)}{dy} = A \cdot B \frac{d\sigma(NN \rightarrow hX)}{dy} \quad (1)$$

However at existing energies the right-hand side of this expression is significantly smaller due to energy conservation corrections. The values of these corrections depend on the classes of multiple scattering diagrams which are taken into account. This problem was analysed in [20] and the results obtained in the so-called rigid target approximation [21, 22] were in agreement [22] with the low energy (~ 4 GeV per nucleon) experimental data on heavy ion collisions.

Rigid target approximation corresponds to the account for the contributions of diagrams shown in Fig. 1. Every nucleon of a beam nucleus A can interact several times with a target nucleus B , however every nucleon of B nucleus can interact only one time. This asymmetrical picture seems to be reasonable for nucleus A fragmentation, because the main part of shadow corrections is accounted for. For fragmentation of nucleus B the result seems to be inconsistent. So the inclusive spectrum of secondary h from AB

collision can be written [20] as

$$\begin{aligned} \frac{1}{\sigma_{AB}^{prod}} \frac{d\sigma(AB \rightarrow hX)}{dy} &= \theta(y) R_A^h(y) \langle N_A \rangle \frac{1}{\sigma_{NB}^{prod}} \frac{d\sigma(NB \rightarrow hX)}{dy} + \\ &+ \theta(-y) R_B^h(-y) \langle N_B \rangle \frac{1}{\sigma_{NA}^{prod}} \frac{d\sigma(NA \rightarrow hX)}{dy}, \end{aligned} \quad (2)$$

where y is the rapidity of secondary h in c.m.s., $\langle N_A \rangle$ and $\langle N_B \rangle$ are the averaged numbers of participating nucleons for every incident nuclei and the functions $R_{A,B}^h(y)$ account for the energy conservation effects. These last quantities can be found from the calculated inclusive spectra in NA and NB collisions, and they differ from unity about 20% at CERN SpS energy and about 10% at RHIC energy.

Now we have to calculate the inclusive cross sections of secondary particle h in NA and NB collisions. It can be done with the help of the quark–gluon string model (QGSM) [15, 16]. This model is based on the Dual Topological Unitarization (DTU) and it describes quite reasonably many features of high energy production processes including the inclusive spectra of different secondary hadrons, their multiplicities, KNO–distributions, etc., both in hadron–nucleon and hadron–nucleus collisions [15, 16, 23].

High energy interactions are considered in QGSM as proceeding via the exchange of one or several pomerons and all elastic and inelastic processes result from cutting through or between pomerons [24]. The possibility of exchanging a different number of pomerons introduces absorptive corrections to the cross sections which are in agreement with the experimental data on production of hadrons consisting of light quarks.

Each pomeron corresponds to a cylindrical diagram, Fig. 2a, and thus, when cutting a pomeron two showers of secondaries are produced (Fig. 2b). The inclusive spectra of secondaries are determined by the convolution of diquark, valence and sea quark distributions $u(x, n)$ in the incident particles and the fragmentation functions $G(z)$ of quarks and diquarks into secondary hadrons. Both the initial quark distributions and the fragmentation functions of quarks and diquarks are constructed using the reggeon counting rules [25].

The diquark and quark distribution functions depend on the number n of cut pomerons in the considered diagram. In the following we use the formalism of QGSM. In the case of a nucleon target the inclusive spectrum of a secondary hadron h (its rapidity, y , or Feynman- x distribution) has the form [15]:

$$\frac{dn}{dy} = \frac{1}{\sigma_{inel}} \frac{d\sigma}{dy} = \frac{x_E}{\sigma_{inel}} \frac{d\sigma}{dx_F} = \sum_{n=1}^{\infty} w_n \phi_n^h(x), \quad (3)$$

where the functions $\phi_n^h(x)$ determine the contribution of diagrams with n cut pomerons and w_n is the probability of this process. Here we neglect the contributions of diffraction dissociation processes which are comparatively small in most of the processes considered below. It can be accounted for separately [15].

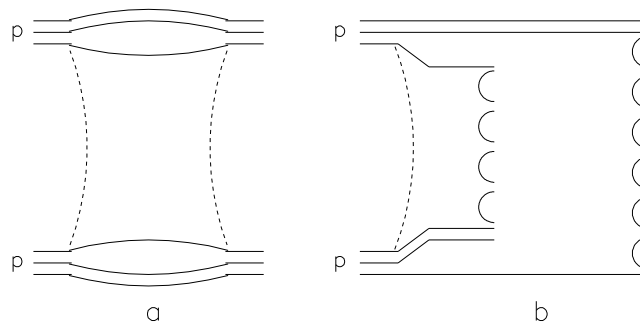


Figure 2: Cylindrical diagram which corresponds to the one-pomeron exchange contribution to elastic pp scattering (a) and its cut which determines the contribution to inelastic pp cross section (b).

For pp collisions

$$\phi_{pp}^h(x) = f_{qq}^h(x_+, n)f_q^h(x_-, n) + f_q^h(x_+, n)f_{qq}^h(x_-, n) + 2(n-1)f_s^h(x_+, n)f_s^h(x_-, n) \quad , \quad (4)$$

$$x_{\pm} = \frac{1}{2}[\sqrt{4m_T^2/s + x^2} \pm x] \quad , \quad (5)$$

where f_{qq} , f_q and f_s correspond to the contributions of diquarks, valence and sea quarks respectively. They are determined by the convolution of the diquark and quark distributions with the fragmentation functions, e.g.,

$$f_q^h(x_+, n) = \int_{x_+}^1 u_q(x_1, n)G_q^h(x_+/x_1)dx_1 \quad . \quad (6)$$

The diquark and quark distributions as well as the fragmentation functions are determined from Regge intercepts. Their expressions are given in Appendix.

The calculation of the inclusive spectra on nuclear targets is similar to Eq. (3). The only difference is that in the case of interaction, say, with three target nucleons and with exchange by five pomerons, it is necessary to account for all possible permutations.

The multiplicities of the produced secondaries can be obtained by integrating the inclusive spectra.

3. Comparison with data

Many examples of the QGSM description of experimental data can be found in [15, 16, 23, 26, 27]. Now we are more interested in particle yields in central (mid-rapidity) region. The data on secondary π^{\pm} and K^{\pm} production in pp collisions at ISR energies [28] at 90° in c.m.s. are presented in Figs. 3a and 3b. We slightly change the pomeron theory parameters, namely its intercept was assumed to be $\alpha_P(0) = 1 + \Delta$ with $\Delta = 0.09$. This values of Δ results in slightly better description of the ISR data. It is practically the same as Donnachie–Landshoff [29] value $\Delta = 0.08$ and rather smaller than the value $\Delta = 0.17$ which was obtained in [30]. The description of secondary protons and antiprotons can be found in [26]. One can see that these data are described by QGSM quite reasonably.

Now we can consider the secondary production in heavy ion collisions. The results of calculations of inclusive density of charged secondaries in mid-rapidity region for CERN SpS energy are in agreement with the data, whereas for RHIC energies are more than two times larger than the RHIC experimental data, and it is impossible to change QGSM parameters to have significantly better description for both pp and heavy ion cases.

This disagreement is rather expected. At comparatively low energies (not higher than several GeV per nucleon) the heavy ion collisions can be considered with the help of standard Glauber approximation, and the inclusive spectrum of any secondary h produced in the central (mid-rapidity) region is described by the diagram shown in Fig. 4a, i.e. by the contribution of a single nucleon-nucleon blob. This diagram immediately

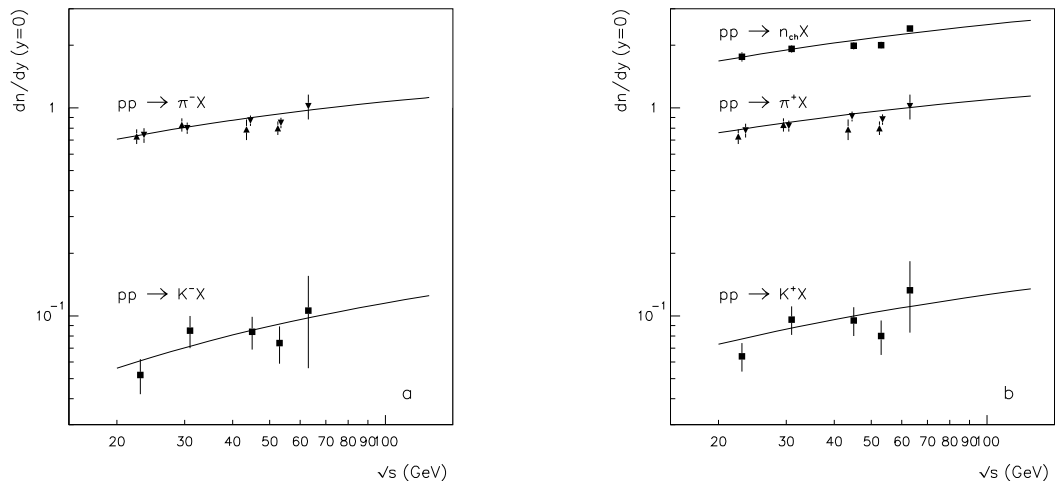


Figure 3: Secondary negative (a) and positive (b) pion and kaon yields at ISR energies [28] at 90° in c.m.s. together with the data for all charged secondaries and with QGSM predictions.

gives Eq. (1) for heavy ion inclusive cross section. The contributions of all other diagrams cancel each other due to AGK cutting rules [24].

At high energies the new diagrams appear which include the interactions of pomerons. The simplest example of such diagrams is so-called triple-pomeron diagram which describe the diffractive production of a large mass M jet in pp interactions. At low energies the contribution of such diagrams to hadron-nucleus or nucleus-nucleus interaction is suppressed by the longitudinal part of nuclear form factor [8]

$$F_A(t_{min}) \approx \exp(R_A^2 t_{min}/3) \quad (7)$$

for Gaussian distribution of nuclear density, where

$$t_{min} \approx (m_N M^2/s)^2. \quad (8)$$

When energy becomes high enough, the value of t_{min} becomes very small. So the discussed contribution can be significant and namely these diagrams determine the inelastic screening corrections to hadron-nucleus cross sections.

One example of a diagram with pomeron interaction for heavy ion interaction is shown in Fig. 4b. Contrary to hadron-nucleus case the contribution of such diagram can be estimated from the processes of high mass jet production in mid-rapidity region and with two large rapidity gaps, see for example Fig. 4c. The numerical contribution of all

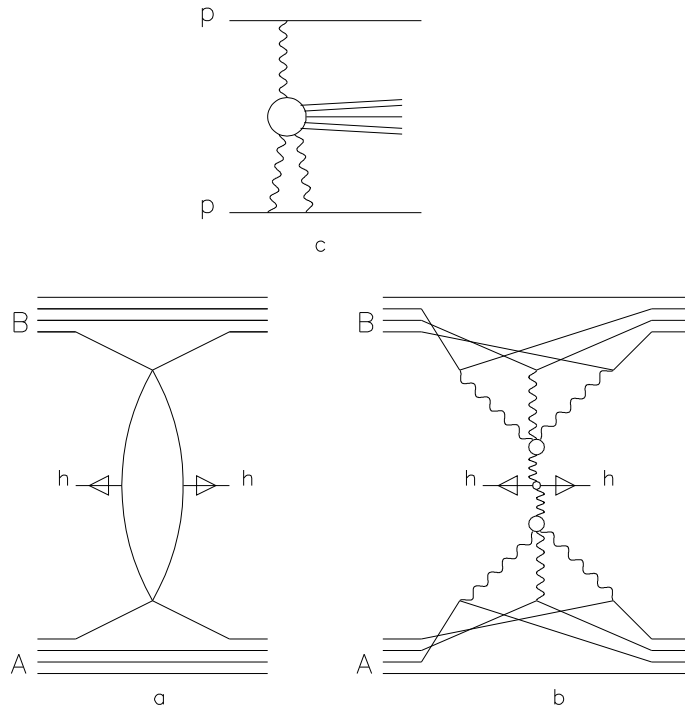


Figure 4: Diagrams for inclusive cross sections for nucleus A -nucleus B collisions in Glauber approximation (a) and with accounting for the interactions of pomerons (shown by wave curves) (b). An example of inelastic processes of pp interactions which determine one of the needed vertices of the multipomeron interactions (c).

such diagrams is rather unclear because the number of diagrams is very large and the vertices of multipomeron interactions are unknown. For example, in [8] the Shwimmer model was used for the numerical estimations. However all such estimation are model dependent.

The numerically significant contribution of the considered diagrams to inclusive density is suppressed quadratically, by both longitudinal form factors, $F_A(t_{min})$ and $F_B(t_{min})$. So we can observe their influence at energies quadratically higher in comparison with the energies region where the inelastic screening effects are observed in hadron-nucleus scattering. One can see that the RHIC energies are of the needed order of magnitude.

The reasonable possibility to estimate the contribution of the diagrams with pomeron interaction comes from percolation theory. We assume that if two or several pomerons are overlapping, they become one pomeron. It means that the inclusive density is saturated, it reaches its maximal value at given impact parameter. This approach has one free parameter - the critical number of pomerons in one squared fermi. Technically it is more simple to bound the maximal number of pomerons, n_{max} , which can be emitted by one participating nucleon for the given pair of colliding nuclei. All model calculations become rather simple because above the critical value every additional pomeron cannot contribute to the inclusive spectrum.

The Dual String Model on the other hand is based essentially on Dual Parton Model ideas [31] with the inclusion of strings [11] which may interact in the transverse plane and fuse, thus reducing their contribution to the final state. Hadrons are considered as made up of constituent quarks (valence and sea quarks): the valence-valence diagram corresponds to single inelastic scattering and the wounded nucleon model [32], while the sea-sea diagram (including gluons) corresponds to additional inelastic multiple scattering contributions. These contributions may be internal, parton multiple scattering within the original valence-valence contribution, or external, involving other nucleons. It should be noticed that the DSM applies only to symmetrical collisions ($A=B$).

The main equation of the DSM was originally written for the rapidity particle density as

$$\left. \frac{dN}{dy} \right|_{N_A N_A} = N_A [2 + 2(k - 1)\alpha] h + (\nu - N_A) 2k\alpha h, \quad (9)$$

where h is the height of the rapidity plateau for valence-valence collisions, αh the height of the sea-sea plateau, $2k$ the average number of strings produced in a nucleon-nucleon collision and N_A is the number of participating nucleons from nucleus A ; finally ν is the average number of nucleon-nucleon collisions, which from elementary multiple scattering arguments [33] satisfies at high energy $\nu \sim N_A^{4/3}$. Notice that the first term on the right-hand side is exactly N_A multiplied by the contribution of one nucleon-nucleon collision, while the second term results from sea-sea type collisions. One should notice that the number of nucleon-nucleon collisions is $N_A + (\nu - N_A) = \nu$ and the number of strings is $N_A [2 + 2(k - 1)] + (\nu - N_A) 2k = 2k\nu$. Assuming that h and α are energy independent (constant plateaus) the energy dependence of $dN/dy|_{pp}$, taken in this model

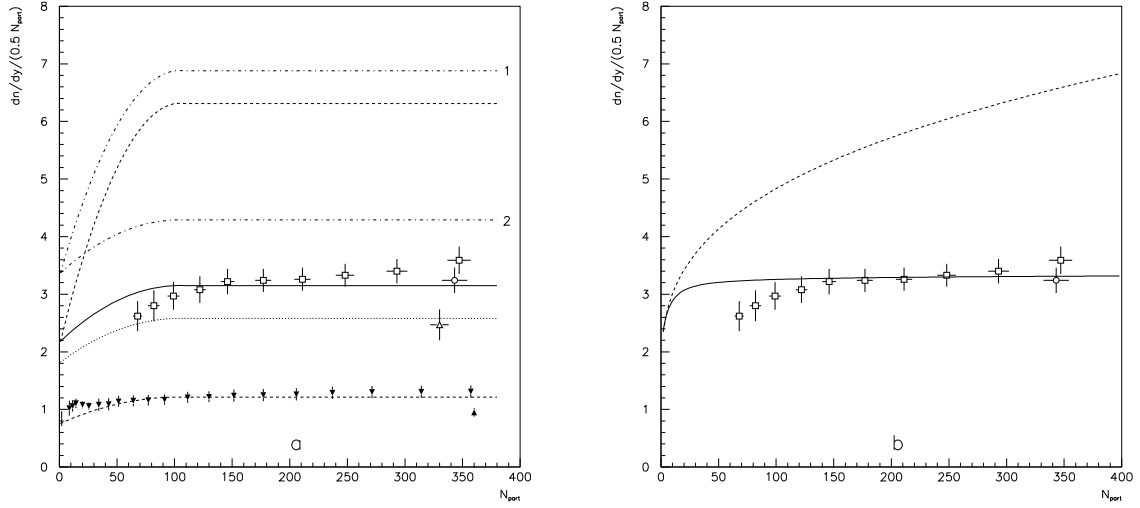


Figure 5: Relative inclusive densities of secondaries for $Pb - Pb$ collisions at $\sqrt{s} = 17.3$ GeV per nucleon (black points, [34, 35, 36], multiplied by 1/2) and for $Au - Au$ at $\sqrt{s} = 130$ GeV per nucleon (open points, [36, 37]) and at $\sqrt{s} = 56$ GeV per nucleon (open triangle, [36]). In Fig. 5a the solid curve shows the results of calculations accounting for the interactions of pomerons with $n_{max} = 1.67$. Dashed curves present the results of the Glauber approximation (without percolation effects) for $\sqrt{s} = 17.3$ GeV per nucleon (lower curve) and $\sqrt{s} = 130$ GeV per nucleon (upper curve). Dotted curve shows our predictions for $Au - Au$ at 56 GeV per nucleon with $n_{max} = 1.67$, and dash-dotted curve 1 and 2 for $Pb - Pb$ collisions at 5.5 TeV per nucleon with $n_{max} = 1.67$ and $n_{max} = 1$, respectively. In Fig. 5b the results of DSM calculations at $\sqrt{s} = 130$ GeV per nucleon with and without string fusion are shown by solid and dashed curves.

by interpolating experimental data, fixes the energy dependence of k , as explained in ref. [9], where it was found that $\alpha = 0.05$ and $h = 0.75$; all results of the DSM shown in this paper are obtained with such values.

By integrating Eq. (9) over the whole rapidity interval predictions are obtained from the DSM for the average multiplicity: the model's result is clearly linear but it overestimates the data. As argued in [17], the assumption that the sea-sea plateau is proportional to the valence-valence plateau is not valid in the fragmentation region, effectively one can say that $\alpha = 0$ there. Fitting the experimental data allows us to estimate that Eq. (9) is valid over the central region corresponding to 70% of total phase space.

The results of calculations of the inclusive densities of the produced charged secondaries per one pair on interacting nucleons $dn_{ch}/dy/(0.5N_{part})$, where $N_{part} = N_A$ with the help of Eq. (2) and QGSM are shown in Fig. 5a. We present the experimental data for $Pb - Pb$ collisions at $\sqrt{s} = 17.3$ GeV per nucleon [34, 35, 36] for $|y| < 1$ and for $Au - Au$ at $\sqrt{s} = 130$ GeV per nucleon [36, 37] and at $\sqrt{s} = 56$ GeV per nucleon for $|\eta| < 1^2$. One can see that CERN SpS data are described reasonably without any additional screening (percolation). It was shown also in [4] and it seems to be natural because the suppression effects of t_{min} discussed above should be rather large at comparatively small energy of CERN SpS.

However, the same calculation at RHIC energy $\sqrt{s} = 130$ GeV per nucleon gives the relative inclusive density two times larger (upper dashed curve in Fig. 5a) than the data, that is in numerical agreement with [8]. The agreement with the data can be obtained only with suppression of multipomeron contributions, namely by using $n_{max} = 1.67$ for every interacting nucleons. The results of DSM calculations with and without string fusion are shown in Fig. 5b, and they are in agreement with the curves in Fig. 5a.

The same value of $n_{max} = 1.67$ allows us to describe the PHOBOS point at 56 GeV (dotted curve in Fig. 5a). In the case of LHC energy $\sqrt{s} = 5.5$ TeV per nucleon for $Pb - Pb$ collisions with $n_{max} = 1.67$ percolation effect decreases the relative inclusive density about 3 times (again similar to [8] prediction). The recent result of PHOBOS Coll. [38] for central $Au - Au$ collisions at $\sqrt{s} = 200$ GeV per nucleon gives $dn_{ch}/d\eta = 650 \pm 35$ for $|\eta| < 1$ that is in agreement with our result $dn_{ch}/d\eta \approx 600$.

However, the percolation effect at LHC energy can be even larger. The transverse range of a pomeron increases with incident energy as

$$r_P^2 \sim \alpha' \ln s/s_0, \quad (10)$$

that is well-known experimentally from the shrinkage of slope parameter in elastic hadron-nucleon scattering. So in the percolation picture the value of n_{max} at higher energies should decrease. The predictions for the relative inclusive density at LHC energy with $n_{max} = 1$ (maximal percolation) are shown in Fig. 5a by dash-dotted curve 2. Now the percolation effect decreases the relative inclusive density about 5 times.

²We accounted for the difference between rapidity and pseudorapidity distributions.

Let us note that Eq. (2) predicts independence of $dn_{ch}/dy/0.5N_A$ on the N_A value for N_A larger than $\langle N_A \rangle$, that is confirmed by the data³. Really some rather weak dependence can exist because in central collisions every participating nucleon interacts more "centrally" on the average in comparison with minimum bias events. However this numerically small effect ($\sim 10\text{-}20\%$ [39]) should be practically suppressed by percolation effects except of rather peripheral collisions, where the value of N_{part} is small and percolation effects are not so important.

The same calculations in the framework of DSM gives similar results as it is shown in Fig. 5b for PHENIX data at $\sqrt{s} = 130$ GeV. Notice that contrary to the case of QGSM approach with Eq. (2) there is no saturation with the number of participants without string fusion.

In Fig. 6 we present the calculated values of the relative inclusive density for secondary production in pp and $Pb - Pb$ collisions as the functions of initial energy. One can see that due to percolation of pomerons emitted by different nucleons with similar impact parameters, the relative inclusive density in $Pb - Pb$ collisions can be smaller than in the pp case. In the case of DSM model the growth with energy is more pronounced than in the QGSM due to the extrapolation of pp data with the second power of $\log s$.

Now let us consider the data [40] on the total number of charged particles detected within range $-5.4 < \eta < 5.4$, i.e. in the region which exclude only high fragmentation and diffraction regions.

These data are in good agreement (Fig. 7) with our calculations in both QGSM and DSM including pp point. Our curves are very close to a straight line, again due to Eq. (2) for QGSM case.

In [40] it was observed also the difference in η -distributions for the central and peripheral $Au - Au$ collisions. Qualitatively the same difference for rapidity distributions of charged secondaries produced in pp and $Au - Au$ collisions at $\sqrt{s} = 130$ GeV per nucleon is presented in Fig. 8. Some shoulder in the dashed curve is connected with secondary proton contribution. It is an artifact of our approach, because we assume that all secondaries have the transverse momenta equal to their averaged values.

The observed differences for rapidity distributions and their numerical values are rather important. They should be connected [41] with the possibility of multiple interactions of every nucleon in heavy ion collision.

4. Conclusions

Immediately after the first data of RHIC and their comparison with CERN SpS data we see for the first time in high energy physics the pomeron (secondary particle) density saturation (percolation effects or contribution from pomeron interactions).

³In the presented approach we can calculate inclusive density for N_A smaller than $\langle N_A \rangle$ only in DSM.

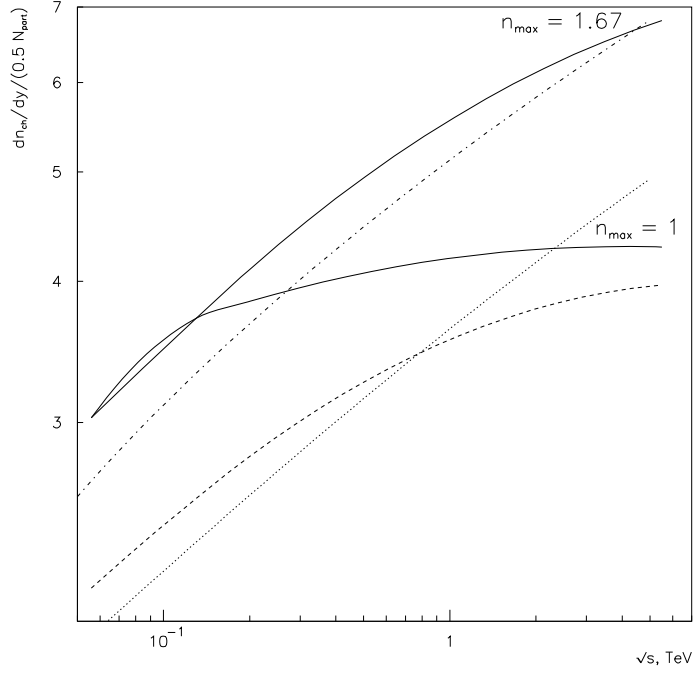


Figure 6: Predictions for the relative inclusive charged particles density for secondaries within range $|y| < 1$ in pp (dashed curve, QGSM and dotted curve, DSM) and $Pb - Pb$ (solid curve, QGSM and dash-dotted curves, DSM) collisions as the functions of initial energy. Two variants of solid curve correspond to percolation effects with $n_{max} = 1.67$ independently on energy and to its decrease from $n_{max} = 1.67$ to $n_{max} = 1$.

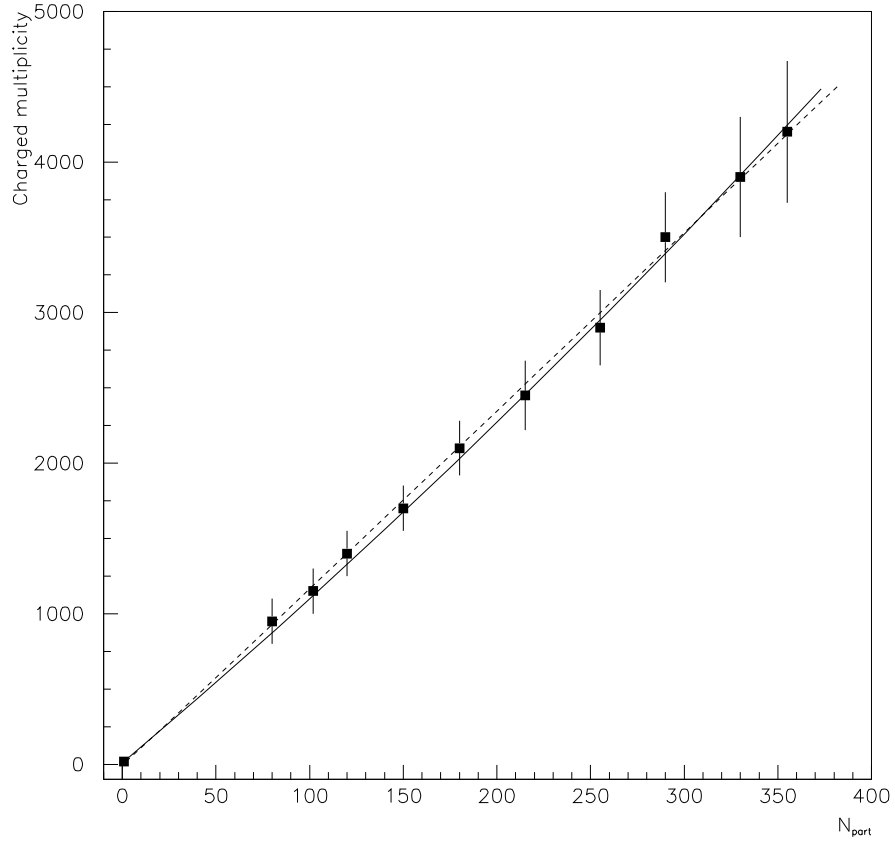


Figure 7: Total number of charged particles detected within range $-5.4 < \eta < 5.4$ in $Au - Au$ collisions at $\sqrt{s} = 130$ GeV per nucleon [40] as a function of N_{part} and its description by the QGSM with percolation effects and $n_{max} = 1.67$ (solid curve) and DSM with string fusion (dashed curve).

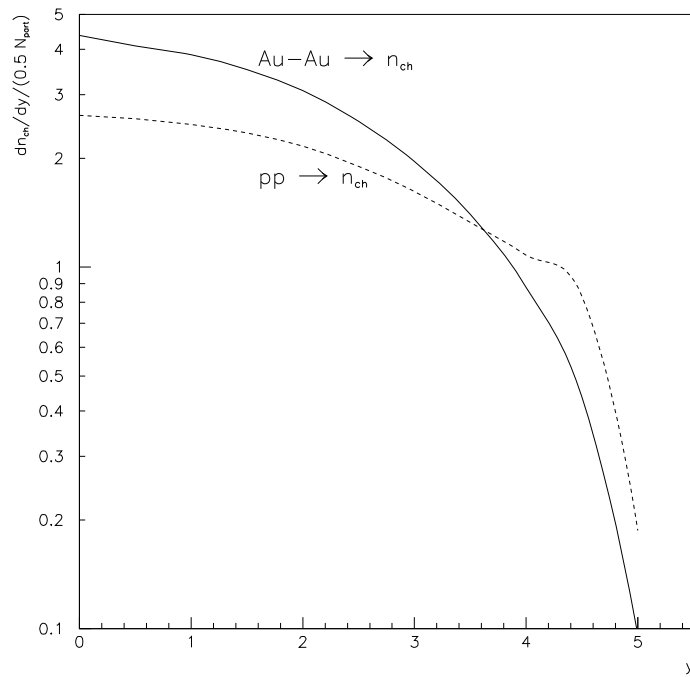


Figure 8: Predicted by QGSM relative rapidity distributions of charged secondaries produced in $Au - Au$ (solid curve) and pp (dashed curve) collisions at $\sqrt{s} = 130$ GeV per nucleon.

With accounting for this new effects with the help of simplest estimations and having only one free parameter (n_{max} – the maximal number of pomerons emitted by one nucleon) we can reproduce many features, observed experimentally in heavy ion collisions. We predict the independence of relative inclusive density $dn_{ch}/dy/(0.5N_{part})$ in the interval between minimum bias and central collisions, i.e. for $A/2 < N_{part} < 2A$ [39], as it is shown in Fig. 5 for mid-rapidity events. We describe the same behaviour ($n_{ch} \sim N_{part}$, Fig. 6) for averaged multiplicities practically in all rapidity region. We reproduce the qualitative difference between the central and peripheral (or pp) heavy ion collisions.

However the discussed new data show some problems for our approach. It seems the most important are rather small ratios of antibaryon to baryon in mid-rapidity region. For example, the ratio of \bar{p}/p yield in the central region is about 0.6 whereas our approach predicts about 0.85 in agreement with calculations of [10]. Possibly, the final state interactions [42] can change the situation. In the opposite case it means that we overestimate the contribution of sea quarks in the central region.

We are grateful to N.Armesto for discussions. This paper was supported by grant NATO PSTCLG 977275.

APPENDIX. Quark and diquark distributions and their fragmentation functions in QGSM

In the present calculations we use quark and diquark distributions in the proton given by the correspondent Regge behaviour [15, 25]. In the case of n -pomeron exchange the distributions of valence quarks and diquarks are softened than in the case of one-pomeron exchange due to the appearance of sea quark contribution. Also it is necessary to account that d -quark distribution is more soft in comparison with u -quark one. There is some freedom [16] how to account for these effects. We use the simplest way and write diquark and quark distributions (for $\alpha_R = 0.5$ and $\alpha_B = -0.5$) as

$$u_{uu}(x, n) = C_{uu}x^{\alpha_R-2\alpha_B+1}(1-x)^{\frac{4}{3}(n-1)-\alpha_R}, \quad (11)$$

$$u_{ud}(x, n) = C_{ud}x^{\alpha_R-2\alpha_B}(1-x)^{n-1-\alpha_R}, \quad (12)$$

$$(13)$$

$$u_u(x, n) = C_u x^{-\alpha_R}(1-x)^{n+\alpha_R-2\alpha_B+1}, \quad (14)$$

$$(15)$$

$$u_d(x, n) = C_d x^{-\alpha_R}(1-x)^{\frac{4}{3}(n-1)+\alpha_R-2\alpha_B+1}, \quad (16)$$

$$(17)$$

$$u_{\bar{u}}(x, n) = u_{\bar{d}}(x, n) = C_{\bar{u}}x^{-\alpha_R} \times [(1-x)^{n+\alpha_R-2\alpha_B-1} - \delta/2(1-x)^{n+2\alpha_R-2\alpha_B-1}], \quad n > 1, \quad (18)$$

$$u_s(x, n) = C_s x^{-\alpha_R}(1-x)^{n+2\alpha_R-2\alpha_B-1}, \quad n > 1, \quad (19)$$

where $\delta = 0.4$ is the relative probability to find a strange quark in the sea. The factors

C_i are determined from the normalization condition

$$\int_0^1 u_i(x, n) dx = 1 \quad (20)$$

with sum rule

$$\int_0^1 \sum_i u_i(x, n) x dx = 1 \quad . \quad (21)$$

The fragmentation functions of quarks and diquarks into pions and kaons were changed a little in comparison with Refs. [15, 23] to obtain a better agreement with the existing experimental data. We use the quark fragmentation functions in the form

$$G_u^{\pi^+} = G_d^{\pi^+} = G_d^{\pi^-} = G_{\bar{u}}^{\pi^-} = a_0(1-z)^{\lambda-\alpha_R}(1-0.7z) \quad , \quad (22)$$

$$G_u^{\pi^-} = G_d^{\pi^+} = G_{\bar{d}}^{\pi^-} = G_{\bar{u}}^{\pi^+} = (1-z)G_u^{\pi^+} \quad , \quad (23)$$

$$G_u^{K^+} = G_{\bar{u}}^{K^-} = a_K(1-z)^\lambda \quad , \quad (24)$$

$$G_u^{K^-} = G_d^{K^-} = G_d^{K^+} = G_{\bar{u}}^{K^+} = G_{\bar{d}}^{K^-} = G_d^{K^+} = G_u^{K^+}(1-z)(1-0.95z) \quad , \quad (25)$$

$$G_s^{\pi^-} = G_s^{\pi^+} = G_{\bar{s}}^{\pi^-} = G_{\bar{s}}^{\pi^+} = (1-z)^{\Delta\alpha} G_u^{\pi^-} \quad , \quad (26)$$

$$G_s^{K^-} = G_{\bar{s}}^{K^+} = a_0(1-z)^{\lambda-\alpha_R}(1-0.7z) \quad , \quad (27)$$

$$G_s^{K^+} = G_{\bar{s}}^{K^-} = (1-z)G_s^{K^-} \quad , \quad (28)$$

with

$$\Delta\alpha = \alpha_\rho - \alpha_\phi = 1/2 \quad , \quad \lambda = 2\alpha' < p_t^2 > = 0.5 \quad , \quad a_0 = 0.73 \quad , \quad a_K = 0.24 \quad . \quad (29)$$

Diquark fragmentation functions have the form :

$$G_{uu}^{\pi^+} = a_0(1-z)^{\lambda+\alpha_R-2\alpha_B}(1+2z) \quad , \quad G_{uu}^{\pi^-} = a_0(1-z)^{\lambda+\alpha_R-2\alpha_B+1}(1-0.9z) \quad (30)$$

$$G_{ud}^{\pi^+} = G_{ud}^{\pi^-} = a_0(1-z)^{\lambda+\alpha_R-2\alpha_B}(1-0.9z) \quad , \quad (31)$$

$$G_{uu}^{K^+} = a_K(1-z)^{\lambda+2(\alpha_R-\alpha_B)} \quad , \quad G_{ud}^{K^+} = G_{uu}^{K^+} \frac{1+(1-z)^2}{2} \quad , \quad (32)$$

$$G_{uu}^{K^-} = G_{ud}^{K^-} = a_K(1-z)^{\lambda+2(\alpha_R-\alpha_B)+1}(1-0.95z) \quad . \quad (33)$$

The probability for a process to have n cut pomerons was calculated using the quasi-eikonal approximation [15, 43]:

$$w_n = \sigma_n / \sum_{n=1}^{\infty} \sigma_n \quad , \quad \sigma_n = \frac{\sigma_P}{nz} (1 - e^{-z} \sum_{k=0}^{n-1} \frac{z^k}{k!}) \quad , \quad (34)$$

$$z = \frac{2C\gamma}{R^2 + \alpha'\xi} e^{\Delta\xi} \quad , \quad \sigma_P = 8\pi\gamma e^{\Delta\xi} \quad , \quad \xi = \ln(s/1 \text{ GeV}^2) \quad , \quad (35)$$

with parameters

$$\Delta = 0.09 \quad , \quad \alpha' = 0.21 \text{ GeV}^{-2} \quad , \quad \gamma_{pp} = 2.2 \text{ GeV}^{-2} \quad , \\ R_{pp}^2 = 3.18 \text{ GeV}^{-2} \quad , \quad C_{pp} = 1.35 \quad .$$

References

- [1] C.Pajares and A.V.Ramallo. Phys.Rev. C16 (1985) 2800.
- [2] V.M.Braun and Yu.M.Shabelski. Int.J.Mod.Phys. A3 (1988) 2417.
- [3] N.Armesto and C.Pajares. Int.J.Mod.Phys. A15 (2000) 2019.
- [4] J.Dias de Deus and Yu.M.Shabelski. hep-ph/0107136.
- [5] Yu.M.Shabelski. Yad.Fiz. 51 (1990) 1396.
D.Krpic and Yu.M.Shabelski. Yad.Fiz. 52 (1990) 766; Z.Phys. C48 (1990) 483.
- [6] V.N.Gribov. Sov.Phys.JETP 29 (1969) 483; 30 (1969) 709.
- [7] O.V.Kancheli and S.G.Matinyan. Yad.Fiz. 11 (1970) 1305.
- [8] A.Capella, A.Kaidalov and J.Tran Thanh Van. Heavy Ion Physics 9 (1999) 169.
- [9] J.Dias de Deus and R.Ugoccioni. Phys.Lett. B494 (2000) 53.
- [10] N.Armesto, C.Pajares and D.Sousa. hep-ph/0104269.
- [11] N.S.Amelin, M.A.Braun and C.Pajares. Phys.Lett. B306 (1993) 312; Z.Phys. C63 (1994) 507.
- [12] M.A.Braun and C.Pajares. Phys.Rev.Lett. 85 (2000) 4864.
- [13] G.H.Arakelian, C.Pajares and Yu.M.Shabelski. Z.Phys. C73 (1997) 697.
- [14] V.N.Gribov. Sov.Phys. JETP 26 (1968) 414.
- [15] A.B.Kaidalov and K.A.Ter-Martirosyan. Yad.Fiz. 39 (1984) 1545; 40 (1984) 211.
- [16] A.B.Kaidalov, Yu.M.Shabelski and K.A.Ter-Martirosyan. Yad.Fiz. 43 (1986) 1282.
- [17] J.Dias de Deus and R.Ugoccioni. Phys.Lett. B491 (2000) 253.
- [18] J.Dias de Deus, R.Ugoccioni and A.Rodrigues, Eur.Phys.J. C16 (2000) 537; Phys.Lett. B458 (1999) 402.
- [19] Yu.M.Shabelski. Acta Phys. Polonica B10 (1979) 1049.
- [20] Yu.M.Shabelski. Yad.Fiz. 50 (1989) 149; Z.Phys. C57 (1993) 409.
- [21] G.D.Alkhozov et al. Nucl.Phys. A220 (1977) 365.

- [22] A.P.Gasparian, A.P.Cheplakov and Yu.M.Shabelski. *Yad.Fiz.* 34 (1981) 1328; 39 (1984) 766.
A.P.Gasparian et al. *Yad.Fiz.* 36 (1982) 690.
- [23] Yu.M.Shabelski. *Yad.Fiz.* 44 (1986) 186.
- [24] V.A.Abramovski, V.N.Gribov, O.V.Kancheli. *Yad.Fiz.* 18 (1973) 595.
- [25] A.B.Kaidalov. *Yad.Fiz.* 43 (1986)(1986) 1282; 45 (1987) 902.
- [26] G.H.Arakelyan, A.Capella, A.B.Kaidalov and Yu.M.Shabelski. hep-ph/0103337.
- [27] A.B.Kajdalov and O.I.Piskunova. *Yad.Fiz.* 41 (1985) 1278.
- [28] M.Banner et al., *Phys. Lett.* B41 (1972) 547
B.Alper et. al. *Nucl. Phys.* B100 (1975) 237.
- [29] A.Donnachie and P.V.Landshoff. *Phys.Lett.* B296 (1992) 227.
- [30] P.V.Chliapnikov, A.K.Likhoded and V.A.Uvarov. *Phys.Lett.* B215 (1988) 417;
A.K.Likhoded and O.P.Yushchenko. *Int.J.Mod.Phys.* A6 (1991) 913.
- [31] A. Capella, U.P. Sukhatme, C.I. Tan and J. Trân Thanh Vân, *Physics Reports* 236 (1994) 225.
- [32] A. Białas, B. Bleszyński and W. Czyż, *Nucl.Phys.* B111 (1976) 461.
- [33] N.Armento and C.Pajares, *Int. J. Mod. Phys.* A15 (2000) 2019.
- [34] NA49 Coll. H.Appelshauser et al. *Phys.Rev.Lett.* 82 (1999) 2471;
P.Jones et al. *Nucl.Phys.* A610 (1996) 188c.
- [35] WA98 Coll. M.M.Aggarwal et al. *Eur.Phys.J.* C18 (2001) 651.
- [36] PHOBOS Coll. B.B.Back et al. *Phys.Rev.Lett.* 85 (2000) 3100.
- [37] PHENIX Coll. K.Adcox et al. *Phys.Rev.Lett.* 86 (2001) 3500.
- [38] PHOBOS Coll. B.B.Back et al. nucl-ex/0108009.
- [39] C.Pajares and Yu.M.Shabelski. *Phys.Atom.Nucl.* 63 (2000) 908; hep-ph/9811214.
- [40] PHOBOS Coll. B.B.Back et al. nucl-ex/0106006.
- [41] Yu.M.Shabelski. *Nucl.Phys.* B132 (1978) 491;
V.V.Anisovich, Yu.M.Shabelski and V.M.Shekhter. *Nucl.Phys.* B133 (1978) 477.
- [42] A. Capella and C.-A. Salgado. *Phys. Rev.* C60 (1999) 054906.
- [43] K.A.Ter-Martirosyan. *Phys.Lett.* B44 (1973) 377.